Liraglutide protects against diastolic dysfunction and improves ventricular protein translation

Cody Rutledge[1], Kevin Redding[1], Mabel Lopez[1], Steven Mullett[2], Stacy Wendell[2], Michael Jurczak[3], Eric Goetzman[4], Brett Kaufman[1]

1. Division of Cardiology, Vascular Medicine Institute, Department of Medicine, University of Pittsburgh, Pittsburgh, PA, USA

2. Department of Pharmacology and Chemical Biology, University of Pittsburgh, Pittsburgh, PA, USA

3. Division of Endocrinology and Metabolism, Department of Medicine, University of Pittsburgh School, Pittsburgh, PA, USA

4. Rangos Research Center, Children's Hospital of Pittsburgh, University of Pittsburgh, Pittsburgh, PA, USA

Corresponding Author:

Cody Rutledge

200 Lothrop Street

BST E1241

Pittsburgh, PA 15261

1-412-624-8644

rutledca@pitt.edu

Abstract

Diastolic dysfunction is an increasingly common cardiac issue contributing to heart failure with preserved ejection fraction (HFpEF). Previous works have implicated glucagon-like peptide 1 (GLP-1) receptor agonists as potential therapies for improving diastolic dysfunction and HFpEF outcomes, though the mechanism of these benefits remains unclear. In this study, we investigated cardiac physiologic and metabolic changes in a mouse model of angiotensin II (AngII)-mediated diastolic dysfunction with or without treatment with the GLP-1 analogue liraglutide. We found that AngII-mediated diastolic dysfunction was abrogated by liraglutide therapy based on echocardiographic changes. The improvements to diastolic dysfunction were associated with broad amino acid accumulation in the heart of the AngII+Liraglutide mice that may support protein synthesis to prevent deleterious remodeling. AngII+Liraglutide mice were also found to have peripheral muscle mass loss and increased circulating amino acids, which may suggest peripheral muscle scavenging of amino acids. Therefore, while liraglutide protects against diastolic dysfunction in the short term, long-term studies are needed to evaluate safety profiles of GLP-1 analogues in diastolic disease.

Introduction

Heart failure with preserved ejection fraction (HFpEF) is an increasingly prevalent syndrome in the United States, comprising over half of all heart failure diagnoses (1). While traditional heart failure therapies may help manage the symptoms of HFpEF, there have been no pharmaceutical interventions shown to lower mortality in HFpEF patients (2). HFpEF is typified by signs and symptoms of fluid overload caused by impaired left ventricular relaxation, called diastolic dysfunction (3). Mouse studies of hypertrophy (4) and HFpEF (5,6) have found that treatment with glucagon-like peptide 1 (GLP-1) inhibitors may improve markers of diastolic dysfunction. However, the mechanism underlying GLP-1 agonist effects in the heart remains complicated and unclear (7).

GLP-1 is an incretin hormone released in the intestine that is known to stimulate insulin secretion and lower blood sugar (8,9). GLP-1 receptor agonists, such as liraglutide, improve outcomes in patients with type 2 diabetes mellitus by normalizing blood glucose levels (8,10). Additionally, GLP-1 agonists are known to improve cardiac outcomes in diabetic patients, demonstrating reduced major adverse cardiac events across multiple GLP-1 analogues (11,12). Independent of diabetes, GLP-1 agonists have also been shown to improve cardiac outcomes in mouse models of hypertension (13), hypertrophy (4), HFpEF (5,6) , and myocardial infarction (14). Additionally, GLP-1 agonists have been approved for weight loss independent of diabetic status (15–17). Given the wide application of GLP-1 agonists and the multiple cardiac effects this class of drugs exhibits, a further understanding of GLP-1 agonists effects and possible benefits towards diastolic dysfunction is warranted.

The purpose of this study was to investigate the cardiac metabolic changes in a mouse model with diastolic dysfunction. We implanted mice with angiotensin-II (AngII) pumps for 4 weeks to model diastolic dysfunction, as previously described (18,19). A cohort of AngII mice were treated simultaneously with the GLP-1 agonist liraglutide (Lira). We evaluated these mice for markers of diastolic dysfunction and profiled metabolomic changes to better understand the mechanism underlying GLP-1 targeted therapy in the heart.

Methods

Angiotensin Pump Implantation and Liraglutide Therapy

All mice were bred and housed at the University of Pittsburgh in accordance with IACUC protocols. Mice were kept on a 12-hour light/dark cycle with water and normal chow ad libitum. Eight-week-old male C57BL/6 mice were anesthetized using vaporized isoflurane (3%) and then underwent AngII pump implantation or sham procedure. The hair over the mid back was removed and a sterile skin incision was made in the AngII implantation mice. Using forceps, a small subcutaneous pocket was opened, and an osmotic pump (Alzet, Cupertino CA) was inserted. Pumps were pre-loaded with angiotensin released at a rate of 1.1 mg/kg/day. The incision was closed with 5-0 vicryl dissolvable suture and covered with topical antibiotic ointment. Animals were monitored post-operatively for recovery. Sham mice were anesthetized but received no surgi cal incision or pump placement. The AngII mice were randomly assigned to either no treatment or Lira groups. The Lira group received daily subcutaneous injections Lira at 0.2 mg/kg/day. All animals were treated for a total of 4 weeks.

Echocardiography

Mice were anesthetized using isoflurane (1-3%) delivered by nose cone at baseline (8 weeks old) and four weeks after AngII implantation. Transthoracic echocardiography was performed using a Vevo 3100 imaging systems (Visual Sonics, Toronto, Canada) with a 40MHz probe, as previously described (20). Briefly, animals were maintained at 37°C and electrocardiogram (ECG) monitored using surface limb electrodes. Heart rate was maintained between 400-500 bpm during imaging by adjusting isoflurane concentration. M-mode and B-mode images of the heart were obtained for at least ten cardiac cycles along the parasternal long axis and left ventricular (LV) short axis. M-mode and Doppler imaging were obtained at the apical window. LV end-diastolic diameter, LV end-systolic diameter, septal and free wall systolic and diastolic thickness were measured along the short axis. LV ejection fraction, LV fractional shortening, and corrected LV mass were calculated based on these values according to previously published Vevo-sonic equations (21). Transmitral Doppler imaging was used to calculate E and A waves as well as isovolumic contraction time (IVCT), isovolumic relaxation time (IVRT), and ejection time (ET). Tissue Doppler from the mitral annulus was used to measure E' and A' values. Speckle tracking was performed by analyzing epicardial and endocardial tissue along the parasternal long-axis by utilizing Vevo 3100 VevoStrain software (22). Mean global longitudinal strain rate was automatically calculated during LV filling, and reverse peak global longitudinal strain rate reported (23). Image analysis was performed by a blinded sonographer.

Blood Pressure

Blood pressure was measured in conscious mice by utilizing a non-invasive CODA tail-cuff system (Kent Scientific, Torrington, CT). Mice were placed in a plastic holder and allowed to rest for 5 minutes before undergoing 5 acclimatization cycles immediately followed by 15 blood pressure measurement cycles. Systolic, diastolic, and mean blood pressure were calculated by the CODA software system, and animals were only included in analysis if >50% of blood pressure readings were registered as successful by the system.

Body Composition and Glucose Tolerance Tests

At 12 weeks age, animals from all groups underwent glucose tolerance test and body composition analysis. Mice were fasted for 6 hours before measuring baseline glucose concentrations in whole blood via tail vein as previously described (24). Briefly, D-glucose diluted in saline was administered at 1 g/kg body weight by intraperitoneal (IP) injection and blood glucose concentrations measured every 15 min for 2 hours using Contour blood glucose test strips (Ascensia Diabetes Care US Inc, Parsippany, NJ). Body composition analyses were completed using ^{1}H magnetic resonance spectroscopy (EchoMRI-100H, Houston, TX) for quantification of lean muscle mass, free water, and body fat.

Tissue and Serum Collection

Following the four-week echocardiography, mice were euthanized under isoflurane anesthetic. Cardiac puncture was performed for collection of blood by heparinized syringe, and hearts were then rapidly excised. Tissues were washed with chilled saline and dissected into atria, right ventricle, and left ventricle, then flash frozen in liquid nitrogen or formalin fixed.

Tissue Histology

Kidneys were fixed overnight in 10% formalin (Thermo, #SF100) at 4°C, then washed with PBS and transferred to 70% ethanol at room temperature. After fixation and dehydration, tissues were embedded in paraffin prior to sectioning at 4 µm by the Histology Core at the Children's Hospital of Pittsburgh. Sections were stained with hematoxylin and eosin (H&E) and trichrome stain. Histological evaluation was performed in a blinded fashion at 40x magnification. Images were obtained on a Nikon Eclipse E800 (Nikon, Tokyo, Japan) microscope at 40x magnification. Images were captured via Nikon NIS-elements software and analyzed using ImageJ. To investigate cardiomyocyte size, 50 short-axis cardiomyocytes were measured for diameter.

Metabolomics Analysis

Targeted metabolomic studies were completed for all three groups via liquid chromatography-high resolution mass spectrometry (LC-HRMS) for citric acid cycle and glycolytic metabolites, amino acids, carnitines, and acetyl-CoA. Metabolic quenching and polar metabolite extraction were performed using ice-cold 80% methanol/0.1% formic acid at a ratio of 500 µL per 50 mg of frozen, powdered LV tissue. An internal standard mix containing (D3)-creatinine and (D3)-alanine, (D4)-taurine, and (D3)-lactate (Sigma-Aldrich) was added to the sample lysates for a final concentration of 100 µM. After 3 min of vortexing, the supernatant was cleared of protein by centrifugation at 16,000 × *g*. Cleared supernatant (3 µL) was subjected to online separation and analysis by LC-HRMS. In brief, samples were injected via a Thermo Vanquish UHPLC and separated over a reversed-phase Thermo HyperCarb porous graphite column (2.1 × 100 mm, 3-µm particle size) maintained at 55°C. For the 20-min LC gradient, the mobile phase consisted of the following: solvent A (water/0.1% formic acid) and solvent B (acetonitrile/0.1% formic acid). The gradient was the following: 0–1 min 1% B, increasing to 15% B over 5 min, increasing to 98% B over 5 min, and held at 98% B for 5 min before equilibration to starting conditions. The Thermo ID-X tribrid mass spectrometer was operated in positive and negative ion mode, scanning in full MS mode (two microscans) from 100 to 800 *m/z* at 70,000 resolution with an automatic gain control target of 2×10^{5}. Source ionization setting was 3.0 kV/2.4vkV spray voltage for positive and negative modes, respectively. Source gas parameters were 45 sheath gas, 12 auxiliary gas at 320°C, and 8 sweep gas. Calibration was performed before analysis using the Pierce FlexMix Ion Calibration Solution (Thermo). Alignment and peak area integration were then extracted manually using Quan Browser (Xcalibur ver. 2.7; Thermo

Fisher). Atomic percent enrichment was calculated using the established mass isotopomer multiordinate spectral analysis (MIMOSA) method to remove the natural [^{13}C] abundance background. Data are graphically represented using Clustvis generated heatmaps (25).

Western Blot

Frozen LV tissue was homogenized in lysis buffer containing a protease/phosphatase cocktail (Sigma-Aldrich, St. Louis, MO, #11697498001) and normalized for protein content using a BCA assay (Life Technologies, Carlsbad, CA, #23235). Samples were separated on NuPage 4-12% gradient SDS-PAGE gels (ThermoFisher, Waltham, MA, #WG1403BOX) and transferred onto iBlot nitrocellulose membranes (Invitrogen, #IB301001). Membranes were blocked in 5% milk (non-phosphorylated antibodies) or 5% BSA (phosphorylated antibodies) for 1 hour and then incubated overnight at 4°C with primary antibodies p-S6 (Ser240/244, 1:1000, Cell Signaling, #2215), S6 (1:1000, Cell Signaling, #2217), GAPDH (1:5000, Millipore, St. Louis, MO, #AB2302), p-4EBP1 (Thr37/46, 1:1000, Cell Signaling, #2855), 4EBP1 (1:1000, Cell Signaling, #9644), and P62 (Invitrogen #PA5-20839, 1:1000). Following incubation, membranes were washed with TBS-tween and then probed for 1 hour at room temperature with anti-mouse or anti-rabbit secondary antibodies (Jackson ImmunoResearch, West Grove, PA, #115-035-003 and #115-035-144). Images were obtained by developing on a ChemiDoc XRS imaging system (BioRad, Hercules, CA) and analyzed using ImageJ software (National Institutes of Health, Bethesda, MD).

Puromycin Assay for Protein Synthesis

Thirty minutes prior to animal sacrifice, a cohort of mice from each treatment group was given an IP injection of puromycin (40 nm/g) to assess protein synthesis in the heart (26,27). Hearts were flash frozen and later homogenized and prepared for Western blot analysis as described above. The transfer membrane was blocked with milk then incubated overnight with 1:1000 with PMY-2A4 (Developmental Studies Hybridoma Bank, University of Iowa) followed by 1 hour with anti-rabbit secondary and developed. Whole lane densitometry was analyzed and compared between groups.

Fatty Acid Oxidation (FAO)

Fresh LVs were homogenized in BIOPS buffer (10 mM Ca-EGTA, 0.1 µM calcium, 20 mM imidazole, 20 mM taurine, 50 mM K-MES, 0.5 mM DTT, 6.56 mM MgCl2, 5.77 mM ATP, 15 mM phosphocreatine to pH 7.1) and the lysate centrifuged at 500 g for 5 min to remove debris. FAO reactions consisted of 5 uL of lysate in a total reaction volume of 200 uL containing 200 mM sucrose, 10 mM Tris-HCl, 5 mM KH_2PO_4, 0.2 mM EDTA, 0.5 % fatty acid-free BSA, 80 mM KCl, 1 mM $MgCl_2$, 0.2 mM L-carnitine, 0.1 mM malate, 0.05 mM coenzyme A, 2 mM ATP, 1 mM DTT, and 125 uM of ^{14}C-labeled palmitic acid (PerkinElmer). ^{14}C-labeled products were separated from the reactions by extraction with chloroform/methanol as previously described (28). The rate of fatty acid oxidation (FAO) was normalized to protein concentration.

Statistical Analysis

Data are expressed as mean ± standard error in all figures. A p-value of ≤ 0.05 was considered significant for all comparisons. One-way ANOVA with Tukey's multiple comparisons test was used to compare groups. All statistical analysis was completed using Graphpad Prism 8 software (San Diego, CA).

Results

AngII treated mice develop diastolic dysfunction that can be prevented by Lira therapy

Following four weeks on angiotensin infusion, AngII treated mice developed diastolic dysfunction as measured by Doppler flow analysis of the mitral valve, including decreased E/A and E/E' (Figure 1A). AngII mice also have reduced peak reverse longitudinal strain rate (rLSR) by speckle tracing analysis. These changes were all prevented in the AngII mice treated with Lira. AngII+Lira mice had unchanged E/A, E/E', and rLSR when compared to the sham mice, but significantly improved E/A, E/E', and rLSR when compared to the untreated AngII cohort. There were no significant changes to isovolumic relaxation time (IVRT) between treatment groups. Ejection fraction (EF) was measured as an indicator of systolic function. There was no change in EF between treatment groups (Figure 1B).

AngII causes fibrosis that is partially prevented by Lira Therapy

AngII mice developed cardiac fibrosis as determined by percentage of high-powered field staining blue by Masson Trichrome Staining (Figure 2A). Fibrotic staining remained elevated in the AngII+Lira mice when compared to sham but was significantly lower in the AngII+Lira mice when compared to untreated AngII mice (Figure 2A).

Lira has no effect on AngII-induced blood pressure elevation and hypertrophy

Systolic and diastolic blood pressure (BP) is elevated in the AngII mice compared to sham (Figure 2B). While AngII+Lira mice had elevated diastolic BP compared to the sham group, there was not a significant difference between sham and AngII+Lira systolic BP. AngII+Lira mice have unchanged systolic and diastolic BP compared to the untreated Ang mice. AngII mice developed hypertrophy as noted by significantly large cross-sectional area in the AngII myocytes when compared to sham. There was no significant difference between the Ang and Ang+Lira cohorts.

AngII+Lira mice have lower body weight and lean muscle mass than AngII Mice

While animal body weights were unchanged at 8-weeks (Table 1), there was a significant decrease in 12-week body weight between the AngII+Lira mice compared to sham. While the AngII cohort did not have a significantly lower body weight at 12-weeks, they did have a significant drop in body weight over time when compared to sham mice (Table 1). To quantify the body composition accounting for these changes, mice underwent whole body MRI. There were no significant changes to body fat or body free water composition between groups, but the Ang+Lira mice did have lower total lean muscle mass when compared to sham (Figure 2C).

AngII+Lira mouse hearts have altered amino acid accumulation compared to sham and AngII

To better assess the metabolic changes related to AngII and AngII+Lira treatments, homogenized hearts underwent targeted metabolomic profiling for amino acids, citric acid cycle and glycolytic intermediates, ketones, and carnitines (Figure 3). AngII+Lira mice were found to have dramatic changes to amino acid accumulation. 15 of the 23 amino acids quantified were found to be elevated in the AngII+Lira cohort compared to sham mice and 14 of the 23 amino acids were elevated compared to AngII mice (Supplemental Figure 2). Less dramatic amino acid accumulation was noted in plasma samples of the AngII+Lira mice when compared to sham (6 of 23 amino acids significantly changed, Supplemental Figures 3 and 4) or AngII mice (2 of 23 amino acids.)

Citric acid cycle and glycolytic intermediates were largely unchanged with or without Lira treatment

Less prominent changes were noted when comparing citric acid cycle and glycolytic intermediates. Acetyl CoA was significantly elevated in the AngII cohort compared to sham (Supplemental Figure 2) but normalized to sham levels in the AngII+Lira cohort. AngII mice had altered levels of a few other intermediates (including aspartate, cis-aconitate, succinate, and sedulopheptase 7 phosphate), while AngII+Lira hearts were largely unchanged from the sham cohort (with the exception of hexose and cis-aconitate). Plasma analysis comparing citric acid cycle and glycolytic intermediates was notable only for elevations of cis-aconitate, itaconate, citrate, and ribulose 5-phosphate between AngII and sham mice. There were no significant changes between the AngII+Lira and sham cohorts.

Ketone and carnitine profiles are altered between treatment groups

Acetoacetate levels were elevated in the AngII+Lira mice when compared to both sham and AngII mice (Supplemental Figure 2), while 3-hydroxybutyrate levels were unchanged. Carnitine and propionylcarnitine levels were elevated in the AngII+Lira compared to sham, while acetylcarnitine, butylcarnitine, isovalerylcarnitine, and octanylcarnitine levels were all significantly reduced between the same cohorts. With the exception of 3-hydroxybutyrate, there were no significant changes between sham and AngII+Lira mice by plasma analysis.

AngII+Lira mouse hearts have altered markers of mRNA processing, autophagy, and protein synthesis

To better understand the role of the amino acid accumulation in the heart, we performed Western blot analysis for markers of mRNA translation and autophagy. We found that phosphorylated ribosomal protein S6, which correlates with ribosomal protein translation (29), is elevated in the AngII+Lira mice when compared to sham (Figure 4A). Similarly, we quantified the translation repressor 4EBP1. When 4EBP1 is phosphorylated, it is degraded and allows eIF4E to initiate translation (30). p-4EBP1/4EBP1 is elevated in the AngII mice compared to sham, however, has significantly higher expression in AngII+Lira mice compared to the AngII group (Figure 4A). p62, a receptor protein associated with degradation of ubiquitinated proteins and autophagy (31), is elevated in AngII+Lira mice when compared to both sham and AngII groups (Figure 4B). Finally, to assess protein synthesis, we treated a cohort of mice with the antibiotic puromycin, which incorporates into elongating amino acid chains and can be quantified as a marker of protein synthesis (26). We found that AngII mice had high puromycin incorporation than sham mice (Figure 4C). AngII+Lira mice had significantly higher puromycin incorporation than both the sham and AngII cohorts.

Fatty Acid Utilization is reduced in AngII+Lira Mice

Given prior reports of FAO as a rescue therapy in diastolic dysfunction (18) as well as the subtle changes to carnitine profiles observed in our AngII and AngII+Lira hearts (Figure 3), we assessed FAO in all three groups using radiolabeled palmitate in homogenized hearts. We found that AngII+Lira hearts had significantly reduced oxidation of palmitate to CO_2 compared to sham mice (Figure 5). While there was no change of acid soluble metabolites (ASM), which include small metabolites such as acetyl-CoA and citric acid cycle intermediates between groups. However, when quantifying CO_2 production compared to total FAO (sum of CO_2 and ASM), we found that AngII+Lira mice had lower palmitate oxidation than both sham and AngII mice.

Discussion

AngII infusion is a well-studied mouse model of hypertension that has been associated with a variety of cardiac pathologies, ranging from subtle diastolic dysfunction to systolic heart failure (32–34). Here we show that our AngII treated mice develop diastolic dysfunction validated by multiple echocardiographic modalities with no change to cardiac ejection fraction (Figure 1). These mice have elevated blood pressure and cardiac hypertrophy by histologic evaluation. We found that daily treatment with liraglutide completely prevented diastolic dysfunction caused by AngII treatment, with no significant changes to blood pressure or hypertrophy (Figure 2). A previous murine model found that liraglutide treatment prevented hypertrophy in the heart when treated with a slightly higher dose of AngII (4), though diastolic parameters were not evaluated. Comparable work in the mouse also found that liraglutide therapy improves diastolic dysfunction and pulmonary congestion in a two-hit model of HFpEF utilizing AngII treatment with a high-fat diet (6). Both works note reduced cardiac fibrosis in the liraglutide treated hearts. Our work supports these findings that liraglutide protects against AngII mediated remodeling in the heart.

A novel finding in our study involves the metabolic changes observed in our AngII+Lira cohort. Targeted metabolomic studies of the heart found dramatic accumulation of nearly all amino acids studied. AngII treated mice had a nearly identical amino acid profile compared to the sham group, with the amino acid ornithine as the only significantly changed metabolite. AngII+Lira mice, however, had 15 of 23 amino acids significantly elevated compared to the sham mice and 14 of 23 compared to the AngII cohort. We initially considered that this broad elevation of amino acids represented an increased reliance of amino acids as an energy substrate, particularly given recent interest in branch-chain amino acids (BCAA) as a fuel source in cardiomyopathy and heart failure (35,36). We report significant changes to BCAA's leucine and valine in our AngII+Lira mice; however, recent work on BCAA's in the heart linked BCAA accumulation to increased protein synthesis and hypertrophy (37), leading us to investigate markers of protein synthesis in our model.

We found that phosphorylated S6, a marker of ribosomal activity (29), is elevated in the AngII+Lira mice when compared to the sham group (Figure 4A). Similarly, AngII+Lira mice had increased phosphorylation of the translational repressor protein 4EBP1, which leads to degradation of 4EBP1 and increased mRNA translation (30). Finally, we injected mice with puromycin prior to terminal studies and found that puromycin incorporation is increased in the AngII+Lira compared to both sham and AngII cohorts, suggesting that protein synthesis is increased in the liraglutide treated mice. It should be noted that p-4EBP1 and puromycin incorporation were both elevated in the AngII mice compared to sham, suggesting that AngII alone is driving increased protein synthesis. Increased protein synthesis has been linked to pathologic cardiac hypertrophy (37) and is consistent with the hypertrophic changes seen in our AngII cohort. When treated with liraglutide, protein synthesis is further increased above AngII levels. While we did not see any significant change to hypertrophy in the AngII+Lira mice compared to AngII mice, we did find reduced levels of fibrosis. One possible explanation for the discrepancy between increased protein synthesis and unchanged hypertrophic measurements is that the liraglutide is supporting protein synthesis and turnover in the heart, allowing cardiomyocytes to persevere against the increased afterload related to elevated blood pressure in both treatment groups. This concept is supported by elevated p62, a marker of autophagy, in the AngII+Lira mice (Figure 4B).

The increased protein synthesis and likely turnover observed in the AngII+Lira heart raises questions about the source of amino acids accumulating in the heart. All groups were fed ad libitum with a normal chow diet. Although food intake was not monitored in these mice, we did find that the AngII+Lira mice had a reduced terminal weight when compared to the sham group (Figure 2). Though this may be expected based on the role of Liraglutides as a weight-loss agent (15,38), we did not find any significant changes to body fat or free water in the mice (Table 1). Rather, the decreased weight seems to be driven by a significant loss of lean muscle mass in the AngII+Lira cohort (Figure 2).

The increased protein synthesis observed in the heart and loss of lean muscle mass in the AngII+Lira mice may suggest that circulating amino acids are being preferentially taken up by the heart or scavenged from peripheral muscle. We performed plasma metabolomic studies in all 3 groups and found that the AngII+Lira mice had elevated circulating amino acids (6 of 23 metabolites elevated in AngII+Lira vs sham mice, Supplemental Figures 5 and 6). Regardless of the source of the elevated circulating amino acids, these findings raise concerns about GLP-1 receptor agonists related to sarcopenia and frailty, particularly given the high prevalence of diastolic dysfunction in the community (39) and growing use of GLP-1 therapies (40).

The metabolomic screening of cardiac tissue did implicate less pronounced changes to other metabolites. Though glycolytic and citric acid cycle intermediates were largely unchanged between the treatment groups, one notable finding included a significant accumulation of Acetyl-Coa in the AngII cohort, which was normalized in the AngII+Lira mice. Acetyl-CoA accumulation may lead to feedback inhibition of FAO (41), which has previously been reported in a similar model of diastolic dysfunction (18). Despite restoration of Acetyl-CoA in the Ang+Lira cohort, we were unable to show any restoration of FAO in cardiac homogenates with labeled palmitate (Figure 5). In fact, the AngII+Lira cohort had significantly lower FAO than the sham cohort, and lower oxidation of palmitate to CO_2 when compared the AngII mice.

In summary, the study presented herein demonstrates that Ang treated mice develop diastolic disease through multiple echocardiographic parameters, and that daily liraglutide therapy completely prevents these markers of diastolic dysfunction. These changes occur independently of blood pressure or hypertrophy but are associated with lower myocardial fibrosis. Metabolomic changes found dramatic changes to amino acid accumulation in the hearts of Ang+Lira mice, which may be promoting protein synthesis to support cardiac remodeling against afterload in the presence of angiotensin. However, the liraglutide therapy was also associated with loss of lean muscle mass, which may be deleterious in the long term. Future studies are needed to explore the long-term consequences of GLP targeted therapies, including risk of sarcopenia and frailty. Additional studies exploring the bioenergetic consequences of amino acid build-up, and possibly anaplerotic roles of these metabolites, in this model.

Acknowledgements

CR, MJ, EG, and BK were responsible for conceptualization of these studies. CR designed the methodology and with KR, ML, and SM, performed the investigation. CR, SM, SW, MJ, and EG were responsible for data curation. Formal analyses were performed by CR, SM, SW, MJ, EG, and BK. Visualization was completed by CR, SM, MJ, and EG. CR and BK wrote the manuscript. BK supervised the project and provided resources for its completion. All authors reviewed the final manuscript and are responsible for its integrity.

Sources of Funding

Research reported in this manuscript was supported by: American Heart Association Transformational Project Award 18TPA34230048, NIH Instrument Grant for Advanced High-Resolution Rodent Ultrasound Imaging System 1S10OD023684-01A1, NIH Training Program in Imaging Sciences in Translational Cardiovascular Research 5T32HL129964, and NIH NRSA 1F32HL156428.

Disclosures

None of the authors have financial disclosures or conflicts of interest

References

1. Owan TE, Hodge DO, Herges RM, Jacobsen SJ, Roger VL, Redfield MM. Trends in Prevalence and Outcome of Heart Failure with Preserved Ejection Fraction. *N Engl J Med*. 2006;355(3):251-259. doi:10.1056/NEJMoa052256

2. Kass KS and DA. Unmet Needs in Cardiovascular Science and Medicine: Heart Failure with Preserved Ejection Fraction: Mechanisms, Clinical Features, and Therapies. *CircRes*. 2012;40(6):1301-1315. doi:10.1007/s10439-011-0452-9.Engineering

3. Borlaug BA, Paulus WJ. Heart failure with preserved ejection fraction: Pathophysiology, diagnosis, and treatment. *Eur Heart J*. 2011;32(6):670-679. doi:10.1093/eurheartj/ehq426

4. Li R, Shan Y, Gao L, Wang X, Wang X, Wang F. The GLP-1 analog liraglutide protects against angiotensin II and pressure overload-induced cardiac hypertrophy via PI3K/AKT1 and AMPKa signaling. *Front Pharmacol*. 2019;10(JUN):1-15. doi:10.3389/fphar.2019.00537

5. Nguyen TD, Shingu Y, Amorim PA, Schenkl C, Schwarzer M, Doenst T. GLP-1 Improves Diastolic Function and Survival in Heart Failure with Preserved Ejection Fraction. *J Cardiovasc Transl Res*. 2018;11(3):259-267. doi:10.1007/s12265-018-9795-z

6. Withaar C, Meems LMG, Markousis-Mavrogenis G, et al. The effects of liraglutide and dapagliflozin on cardiac function and structure in a multi-hit mouse model of heart failure with preserved ejection fraction. *Cardiovasc Res*. 2020;256:1-17. doi:10.1093/cvr/cvaa256

7. Al Batran R, Almutairi M, Ussher JR. Glucagon-like peptide-1 receptor mediated control of cardiac energy metabolism. *Peptides*. 2018;100(October 2017):94-100. doi:10.1016/j.peptides.2017.12.005

8. Gaspari T, Brdar M, Lee HW, et al. Molecular and cellular mechanisms of glucagon-like peptide-1 receptor agonist-mediated attenuation of cardiac fibrosis. *Diabetes Vasc Dis Res*. 2016;13(1):56-68. doi:10.1177/1479164115605000

9. Andreasen CR, Andersen A, Knop FK, Vilsbøll T. How glucagon-like peptide 1 receptor agonists work. *Endocr Connect*. 2021;10(7):R200-R212. doi:10.1530/EC-21-0130

10. Koliaki C, Doupis J. Incretin-based therapy: A powerful and promising weapon in the treatment of type 2 diabetes mellitus. *Diabetes Ther*. 2011;2(2):101-121. doi:10.1007/s13300-011-0002-3

11. Husain M, Birkenfeld AL, Donsmark M, et al. Oral Semaglutide and Cardiovascular Outcomes in Patients with Type 2 Diabetes. *N Engl J Med*. 2019;381(9):841-851. doi:10.1056/nejmoa1901118

12. Mann JFE, Nauck MA, Nissen SE, et al. Liraglutide and cardiovascular outcomes in type 2 diabetes. *Drug Ther Bull*. 2016;54(9):101. doi:10.1056/nejmoa1603827

13. Chen P, Yang F, Wang W, et al. Liraglutide Attenuates Myocardial Fibrosis via Inhibition of AT1R-Mediated ROS Production in Hypertensive Mice. *J Cardiovasc Pharmacol Ther*. 2021;26(2):179-188. doi:10.1177/1074248420942007

14. Noyan-Ashraf MH, Abdul Momen M, Ban K, et al. GLP-1R agonist liraglutide activates cytoprotective pathways and improves outcomes after experimental myocardial infarction in mice. *Diabetes*. 2009;58(4):975-983. doi:10.2337/db08-1193

15. Ryan D, Acosta A. GLP-1 receptor agonists: Nonglycemic clinical effects in weight loss and

beyond. *Obesity*. 2015;23(6):1119-1129. doi:10.1002/oby.21107

16. Pi-Sunyer X, Astrup A, Fujioka K, et al. A Randomized, Controlled Trial of 3.0 mg of Liraglutide in Weight Management. *N Engl J Med*. 2015;373(1):11-22. doi:10.1056/nejmoa1411892

17. Astrup A, Carraro R, Finer N, et al. Safety, tolerability and sustained weight loss over 2 years with the once-daily human GLP-1 analog, liraglutide. *Int J Obes*. 2012;36(6):843-854. doi:10.1038/ijo.2011.158

18. Choi YS, de Mattos ABM, Shao D, et al. Preservation of myocardial fatty acid oxidation prevents diastolic dysfunction in mice subjected to angiotensin II infusion. *J Mol Cell Cardiol*. 2016;100:64-71. doi:10.1016/j.yjmcc.2016.09.001

19. Xu Z, Okamoto H, Akino M, Onozuka H, Matsui Y, Tsutsui H. Pravastatin attenuates left ventricular remodeling and diastolic dysfunction in angiotensin II-induced hypertensive mice. *J Cardiovasc Pharmacol*. 2008;51(1):62-70. doi:10.1097/FJC.0b013e31815bb629

20. Rutledge C, Cater G, McMahon B, et al. Commercial 4-dimensional echocardiography for murine heart volumetric evaluation after myocardial infarction. *Cardiovasc Ultrasound*. 2020;18(1):1-10. doi:10.1186/s12947-020-00191-5

21. Zhou Y-Q, Foster FS, Nieman BJ, Davidson L, Chen XJ, Henkelman RM. Comprehensive transthoracic cardiac imaging in mice using ultrasound biomicroscopy with anatomical confirmation by magnetic resonance imaging. *Physiol Genomics*. 2004;18(2):232-244. doi:10.1152/physiolgenomics.00026.2004

22. Bauer M, Cheng S, Jain M, et al. Echocardiographic Speckle-Tracking Based Strain Imaging for Rapid Cardiovascular Phenotyping in Mice. *Circ Res*. 2013;108(8):908-916. doi:10.1038/mp.2011.182.doi

23. Schnelle M, Catibog N, Zhang M, et al. Echocardiographic evaluation of diastolic function in mouse models of heart disease. *J Mol Cell Cardiol*. 2018;114(June 2017):20-28. doi:10.1016/j.yjmcc.2017.10.006

24. Jurczak MJ, Lee HY, Birkenfeld AL, et al. SGLT2 deletion improves glucose homeostasis and preserves pancreatic β-cell function. *Diabetes*. 2011;60(3):890-898. doi:10.2337/db10-1328

25. Metsalu T, Vilo J. ClustVis: A web tool for visualizing clustering of multivariate data using Principal Component Analysis and heatmap. *Nucleic Acids Res*. 2015;43(W1):W566-W570. doi:10.1093/nar/gkv468

26. Ravi V, Jain A, Ahamed F, Fathma N, Desingu PA, Sundaresan NR. Systematic evaluation of the adaptability of the non-radioactive SUnSET assay to measure cardiac protein synthesis. *Sci Rep*. 2018;8(1):1-11. doi:10.1038/s41598-018-22903-8

27. David A, Dolan BP, Hickman HD, et al. Nuclear translation visualized by ribosome-bound nascent chain puromycylation. *J Cell Biol*. 2012;197(1):45-57. doi:10.1083/jcb.201112145

28. Goetzman ES, Bharathi SS, Zhang Y, et al. Impaired mitochondrial medium-chain fatty acid oxidation drives periportal macrovesicular steatosis in sirtuin-5 knockout mice. *Sci Rep*. 2020;10(1):1-14. doi:10.1038/s41598-020-75615-3

29. Peterson RT, Schreiber SL. Translation control: Connecting mitogens and the ribosome. *Curr Biol*.

1998;8(7):248-250. doi:10.1016/s0960-9822(98)70152-6

30. Gingras AC, Kennedy SG, O'Leary MA, Sonenberg N, Hay N. 4E-BP1, a repressor of mRNA translation, is phosphorylated and inactivated by the Akt(PKB) signaling pathway. *Genes Dev*. 1998;12(4):502-513. doi:10.1101/gad.12.4.502

31. Seibenhener ML, Babu JR, Geetha T, Wong HC, Krishna NR, Wooten MW. Sequestosome 1/p62 Is a Polyubiquitin Chain Binding Protein Involved in Ubiquitin Proteasome Degradation. *Mol Cell Biol*. 2004;24(18):8055-8068. doi:10.1128/mcb.24.18.8055-8068.2004

32. Regan JA, Mauro AG, Carbone S, et al. A Mouse Model of Heart Failure with Preserved Ejection Fraction due to Chronic Infusion of a Low Subpressor Dose of Angiotensin II. *Am J Physiol - Hear Circ Physiol*. 2015;23298:ajpheart.00282.2015. doi:10.1152/ajpheart.00282.2015

33. Dai DF, Johnson SC, Villarin JJ, et al. Mitochondrial oxidative stress mediates angiotensin II-induced cardiac hypertrophy and g??q overexpression-induced heart failure. *Circ Res*. 2011;108(7):837-846. doi:10.1161/CIRCRESAHA.110.232306

34. Matsuzaki M, Matsuda S, Murata T, et al. Angiotensin Ⅱ Activates MCP-1 and Induces Cardiac Hypertrophy and Dysfunction via Toll-like Receptor 4. *J Atheroscler Thromb*. 2015;22(8):833-844. doi:10.5551/jat.27292

35. Lopaschuk GD, Ussher JR. Evolving Concepts of Myocardial Energy Metabolism: More Than Just Fats and Carbohydrates. *Circ Res*. 2016;119(11):1173-1176. doi:10.1161/CIRCRESAHA.116.310078

36. Ritterhoff J, Tian R. Metabolismin cardiomyopathy: Every substrate matters. *Cardiovasc Res*. 2017;113(4):411-421. doi:10.1093/cvr/cvx017

37. Walejko JM, Christopher BA, Crown SB, et al. Branched-chain α-ketoacids are preferentially reaminated and activate protein synthesis in the heart. *Nat Commun*. 2021;12(1):1-14. doi:10.1038/s41467-021-21962-2

38. Raun K, Von Voss P, Gotfredsen CF, Golozoubova V, Rolin B, Knudsen LB. Liraglutide, a long-acting glucagon-like peptide-1 analog, reduces body weight and food intake in obese candy-fed rats, whereas a dipeptidyl peptidase-IV inhibitor, vildagliptin, does not. *Diabetes*. 2007;56(1):8-15. doi:10.2337/db06-0565

39. Kuznetsova T, Herbots L, López B, et al. Prevalence of left ventricular diastolic dysfunction in a general population. *Circ Hear Fail*. 2009;2(2):105-112. doi:10.1161/CIRCHEARTFAILURE.108.822627

40. Trujilo J, Nuffer W, Smith B. GLP-1 receptor agonists: an updated review of head-to-head clinical studies. *Ther Adv Endocrinol Metab*. 2021;12:1-15. doi:10.1177/https

41. Schulz H. Regulation of Fatty Acid Oxidation in the Heart. *J Nutr*. 1994;124:165-171.

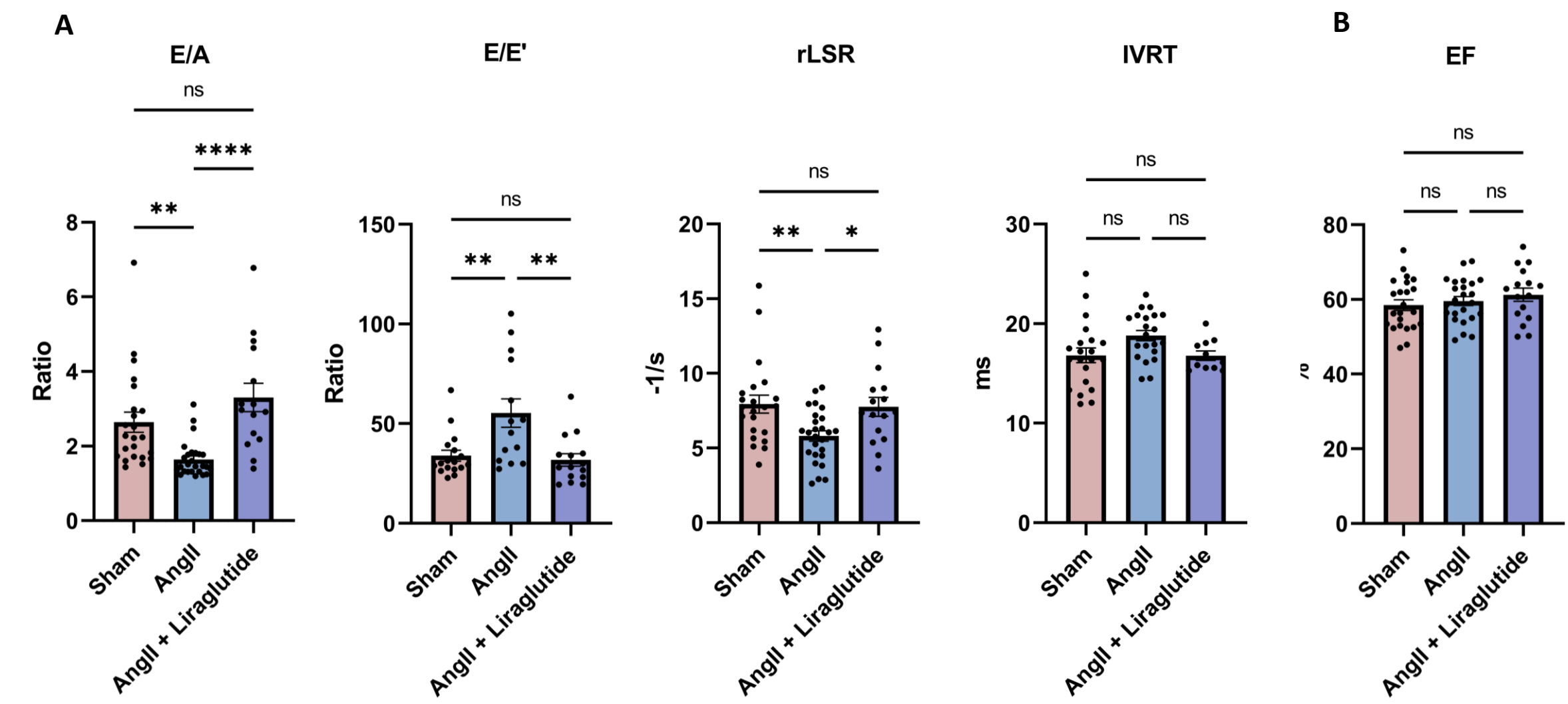

Figure 1. Liraglutide protects against angiotensin (AngII) induced diastolic dysfunction. A) AngII mice (n=14) have evidence of diastolic dysfunction when compared to sham (n=17) as measured by reduced E/A and elevated E/E' by doppler imaging and decreased peak reverse longitudinal strain rate (rLSR) by speckle tracing. E/A, E/E', and rLSR are all normalized in the AngII mice treated with liraglutide (n=15). Isovolumic relaxation time (IVRT) is unchanged between groups. B) Ejection fraction (EF) is unchanged between groups by 2-dimensional imaging. *$p \leq 0.05$, **$p \leq 0.01$, ****$p \leq 0.0001$ by ANOVA with Tukey's multiple comparison test.

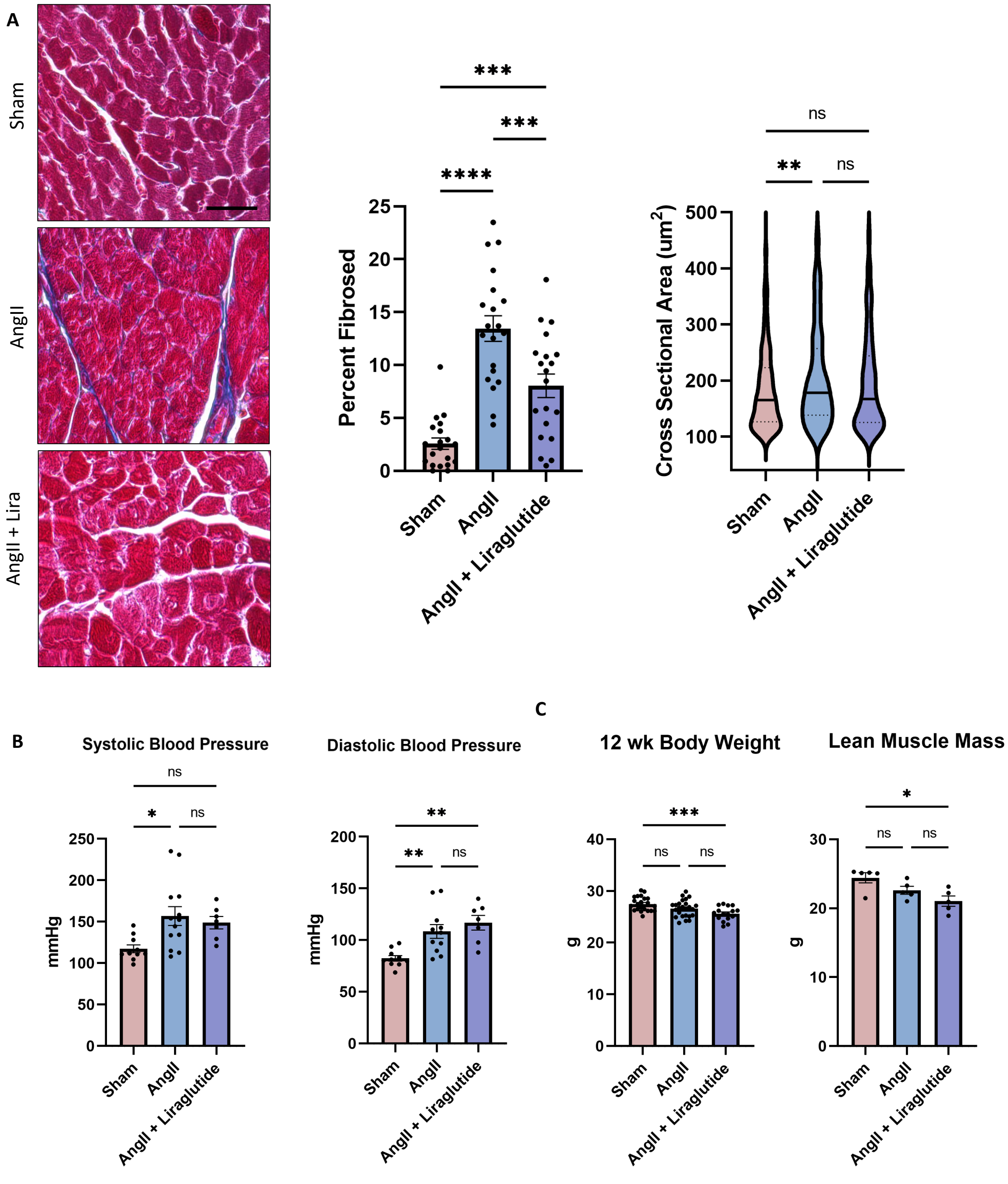

Figure 2. Changes to fibrosis, hypertrophy, blood pressure, and lean muscle mice. A) Left ventricles (LV's) from AngII mice have increased fibrosis by trichrome staining when compared to sham mice. AngII+Liraglutide mice have less fibrosis when compared to AngII mice (n=20 high power fields from 4 mice per group). AngII myocytes have increased cross-sectional area compared to sham that is unchanged in the AngII+Liraglutide mice (n=200-300 myocytes from 4 mice per group). B) Systolic blood pressure is elevated in AngII (n=12) compared to sham (n=10) but not significantly changed in AngII+Liraglutide mice (n=7). Diastolic blood pressure is significantly elevated in both AngII and AngII+Liraglutide mice compared to sham. C) Total body weight and lean muscle mass are decreased in AngII+Liraglutide mice when compared to sham (n=5 per group). *$p \leq 0.05$, **$p \leq 0.01$,***$p \leq 0.001$ ****$p<0.0001$ by ANOVA with Tukey's multiple comparison test. Scale bar = 75 um.

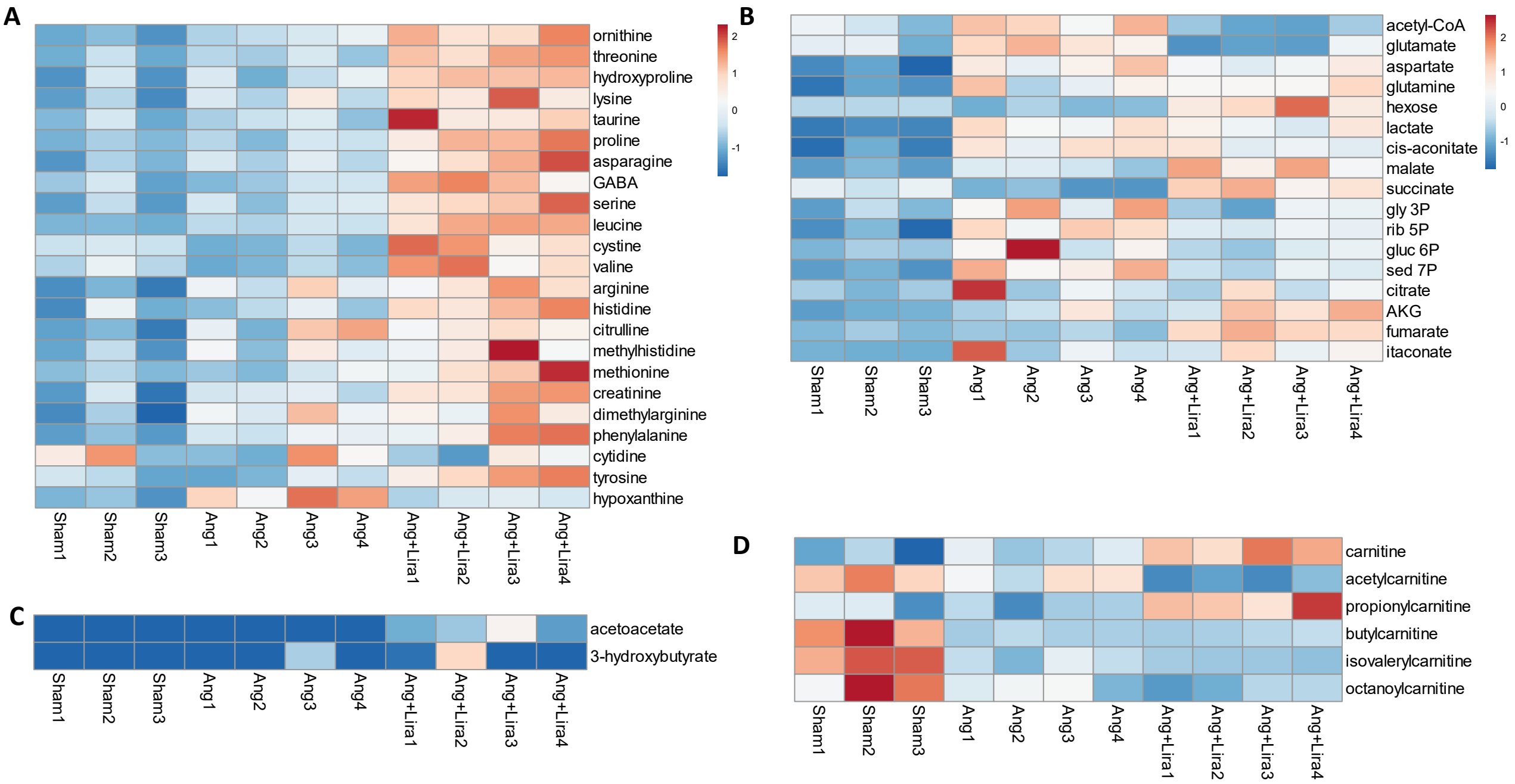

Figure 3. Targeted analysis of amino acids, citric acid cycle and glycolytic intermediates, ketones, and carnitines by metabolomic evaluation. A) AngII+Lira mice demonstrate amino acids accumulation when compared to both Sham and AngII groups Full details available in Supplemental Figure 3 (n=3-4 per group). B) Summary of citric acid and glycolytic intermediates in Sham, AngII, and AngII + Lira groups. C) Summary of ketone accumulation in Sham, AngII, and AngII + Lira groups. D) Summary of carnitine accumulation in Sham, AngII, and AngII + Lira groups.

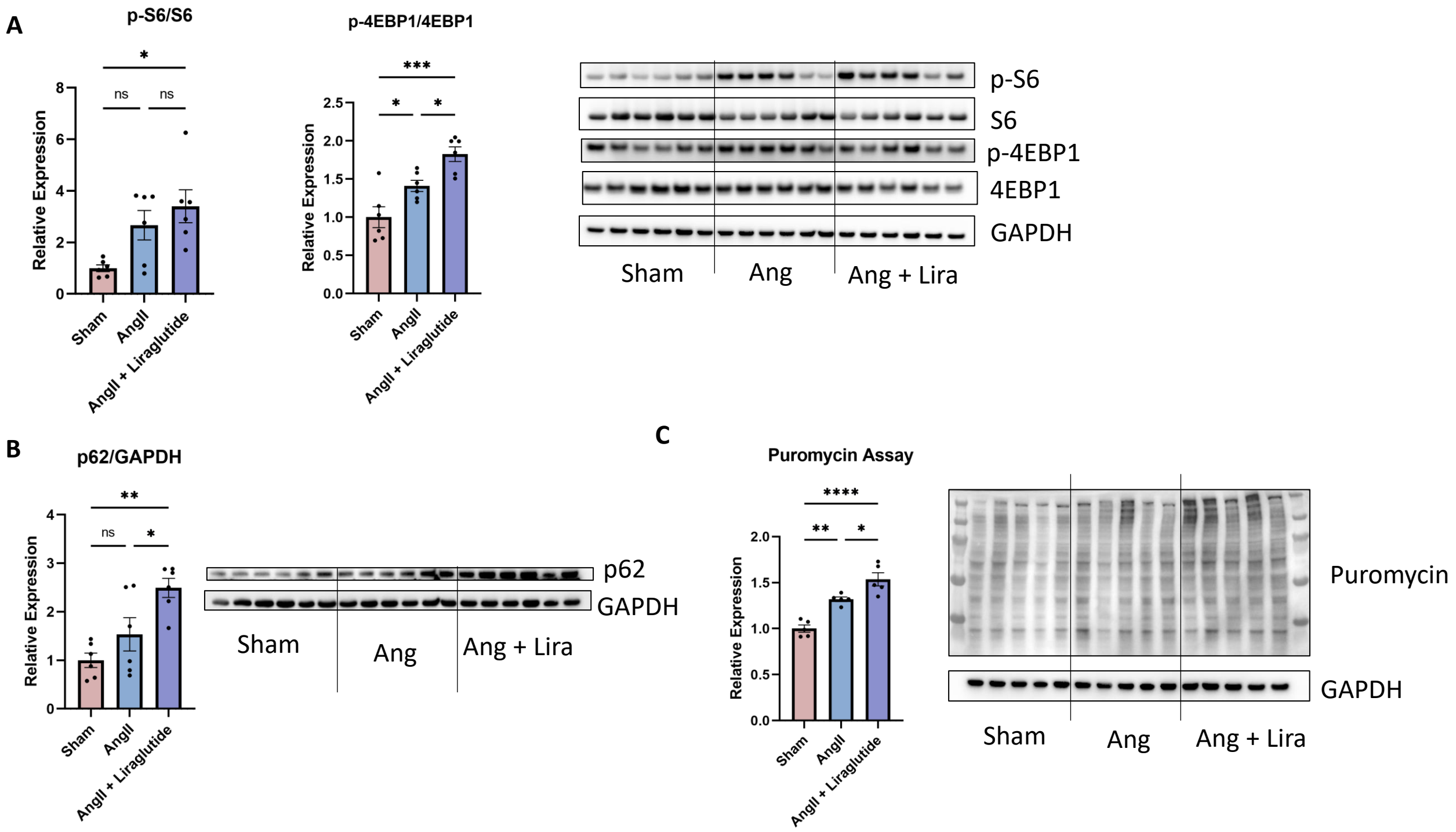

Figure 4. Liraglutide increases markers of mRNA translation and autophagy and promotes protein synthesis in AngII mice. A) AngII mice treated with liraglutide have elevated p-S6/S6 compared to sham mice. AngII mice treated with liraglutide have elevated p-4EBP1/4EBP1 compared to both sham and AngII mice (n=6/group) B) AngII mice treated with liraglutide have elevated p62 compared to Sham and AngII mice (n=6/group). C) Puromycin inclusion is increased in AngII mice treated with liraglutide (n=5/group) when compared to Sham and AngII mice. *$p \leq 0.05$, **$p \leq 0.01$,***$p \leq 0.001$ ****$p \leq 0.0001$ by ANOVA with Tukey's multiple comparison test.

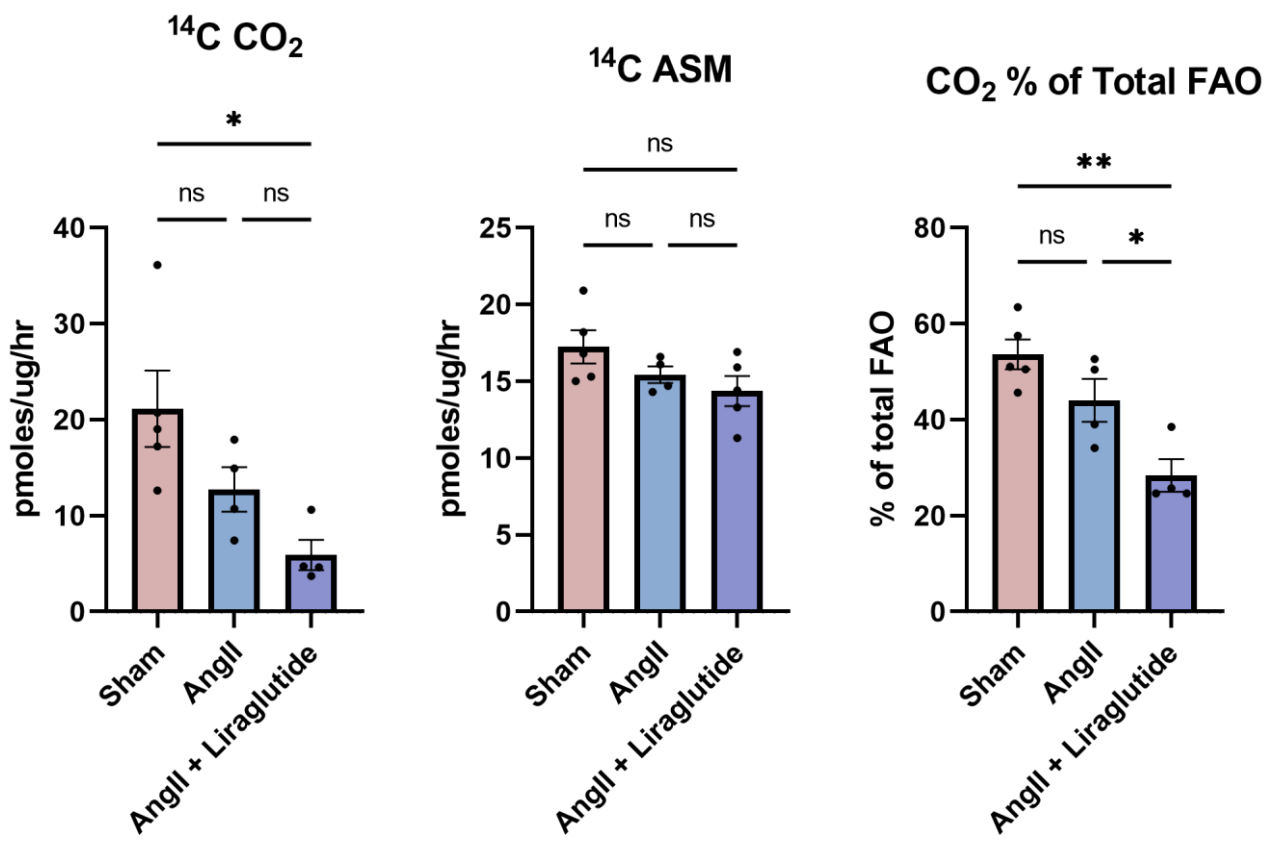

Figure 5. Palmitate oxidation is altered in AngII and AngII + Liraglutide mice. ^{14}C labeled palmitate was given to homogenized hearts in each group to measure fatty acid oxidation (FAO). AngII + Liraglutide mice had significantly less CO2 formation than sham mice. There was no change to acid soluble metabolites (ASM) between groups. CO2 production was significantly lower in the AngII + Liraglutide mice when compared to Sham and AngII when comparing CO2 as a percentage of total palmitate oxidation. n=4/group, *$p \leq 0.05$, **$p \leq 0.01$ by ANOVA with Tukey's multiple comparison test.

	Sham (n=22)	AngII (n=25)	AngII+Liraglutide (n=16)
8-wk Body Weight (g)	24.56±0.28	24.56±0.33	24.34±0.41
12-wk Body Weight	27.49±0.29	26.60±0.32	25.61±0.34*
Delta Body Weight	2.93±0.23	2.04±0.23*	1.27±0.19***
Terminal Random Blood Glucose	163±25	144±25	152±18
Terminal Random Blood Lactate	2.20±0.51	2.65±0.09	2.32±0.26
Terminal Body Fat (g)	1.47±0.18	1.34±0.09	1.55±0.27
Terminal Body Free Water (g)	0.25±0.10	0.19±0.08	0.23±0.04

Table 1. Physiologic characteristics of Sham, AngII, and AngII+Liraglutide mice. At the time of surgery (8-week old mice), there is no change to baseline body weight between Sham (n=22), Ang (n=25), and AngII+liraglutide mice (n=16). 4-weeks after surgery, AngII+liraglutide mice have lower body weight than sham mice. Both AngII and AngII+Liraglutide have lower delta body weights over the 4-week experiment. There is no change to random blood glucose, lactate, body fat, or free water between groups at terminal procedure (n=5/group). *$p \leq 0.05$, ***$p \leq 0.001$ vs sham by ANOVA with Tukey's multiple comparison test.